ELSEVIER

Journal of Marine Systems 16 (1998) 199–217

JOURNAL OF MARINE SYSTEMS

Initial results from long-term measurements of atmospheric humidity and related parameters in the marine boundary layer at two locations in the Gulf of Mexico

Laurence C. Breaker [a,*], David B. Gilhousen [b], Hendrik L. Tolman [a], Lawrence D. Burroughs [a]

[a] *NOAA / National Weather Service, NCEP, Washington, DC 20233-9910, USA*
[b] *NOAA / National Weather Service, National Data Buoy Center, Stennis Space Center, Stennis, MS 39529, USA*

Received 16 August 1996; accepted 8 August 1997

Abstract

Measurements of boundary layer moisture have been acquired from Rotronic MP-100 sensors deployed on two NDBC buoys in the northern Gulf of Mexico from June through November 1993. For one sensor, which was retrieved approximately 8 months after deployment, the post- and precalibrations agreed closely and fell well within WMO specifications for accuracy. The second sensor operated continuously from June 1993 to February 1997 (~ 3.5 years). Buoy observations of relative humidity and supporting data were used to calculate specific humidity and the surface fluxes of latent and sensible heat. Specific humidities from the buoys were compared with observations of moisture obtained from nearby ship reports, and the correlations were generally high (0.7–0.9). Surface gravity wave spectra were also acquired. The time series of specific humidity and the other buoy parameters revealed three primary scales of variability, small (~ h), synoptic (~ days), and seasonal (~ months). The synoptic variability was clearly dominant and occurred primarily during September, October, and November. Most of the synoptic variability was due to frontal systems that dropped down into the Gulf of Mexico from the continental US followed by air masses which were cold and dry. Cross-correlation analyses of the buoy data indicated that: (1) the moisture field was highly coherent over distances of 800 km or more in the northern Gulf of Mexico; and (2) both specific humidity and air temperature served as tracers of the motion associated with propagating atmospheric disturbances. These correlation analyses also revealed that the prevailing weather systems generally entered the buoy domain from the South prior to September, but primarily from the North thereafter. Spectra of the various buoy parameters indicated strong diurnal and semidiurnal variability for barometric pressure and sea surface temperature (SST) and lesser variability for air temperature, wind speed and significant wave height. The surface fluxes of latent and sensible heat were dominated by the synoptic events which took place from September through November with the transfer of latent heat being primarily from the ocean to the atmosphere. Finally, an analysis of the surface wave observations from each buoy, which included calculations of wave age and estimates of surface roughness, indicate that major heat and moisture flux events coincide with periods of active wave growth, although the data were insufficient to identify any causal relationships.

Keywords: Rotronic MP-100 humidity sensors; humidity; marine boundary layer; Gulf of Mexico; latent heat flux; surface waves

* Corresponding author.

PII: S0924-7963(97)00041-9

1. Introduction

Due to the proximity of the ocean surface to the sensor location, and the constant state of motion of the surface itself, the acquisition of meteorological observations within the marine boundary layer has always posed unique problems. Atmospheric humidity has been a particularly difficult parameter to measure near the ocean surface. First, it is difficult to protect humidity sensors from salt spray which accumulates over time and consequently degrades calibration accuracy; second, humidity sensors must be adequately protected from excess heating due to incoming solar radiation; and third, humidity sensors must recover rapidly from periods of saturation without change to their calibration (Coantic and Friehe, 1980).

Since atmospheric moisture is a difficult parameter to measure accurately over the ocean, it is not surprising that it has been even more difficult to acquire observations from unattended instruments for extended periods. Recently, a number of humidity sensors have been evaluated for possible use in measuring atmospheric moisture in the marine environment (e.g. Semmer, 1987; Muller and Beekman, 1987; Crescenti et al., 1990; Katsaros et al., 1994).

Based on promising test results from Muller and Beekman (1987) and Semmer (1987), and because of the continuing need for long-term measurements of moisture within the marine boundary layer, the National Data Buoy Center (NDBC) evaluated the Rotronic MP-100 humidity sensor for possible deployment on their moored ocean data buoys. Initial field tests were conducted along the US West Coast in 1989. A Rotronic humidity sensor was installed on a Coastal-Marine Automated Network (C-MAN) station at Point Arguello, California and showed high correlations between saturation events and restricted visibilities in fog. Calculated dew point temperatures following fog events were in general agreement with those reported at nearby Vandenberg Air Force Base. After a 4-month evaluation, Rotronic humidity sensors were introduced on several NDBC buoys and C-MAN stations along the California coast. Initially, several instrument failures occurred within weeks after installation. These failures led to several improvements to the sensor and its installation. First, the cabling from the sensor to the onboard electronic payload was replaced. The original cables had inadequate insulation, and cable flexing often produced large calibration shifts. Second, the method of calibration was changed by exposing the sensor to a series of different saturated salt solutions in closed flasks and then comparing the observed relative humidities to the known equilibrium vapor pressure of water at the observed temperatures for these solutions. Test flasks with relative humidities ranging from 11 to 96% were used. These modifications led to significantly greater measurement accuracy and sensor reliability. The enhanced instruments have been installed on a number of NDBC buoys, and their performance has steadily improved.

As a basis for this study, we acquired hourly measurements of relative humidity and other supporting environmental data from two NDBC buoys in the Gulf of Mexico (Fig. 1). These buoys were equipped with the improved Rotronic MP-100 humidity sensors for the period 5 June to 30 November 1993. First, details of the sensor calibration, deployment and reliability are addressed. Then the relative humidity and supporting data are used to calculate specific humidity at each buoy location. To provide a measure of validation for these observations, the

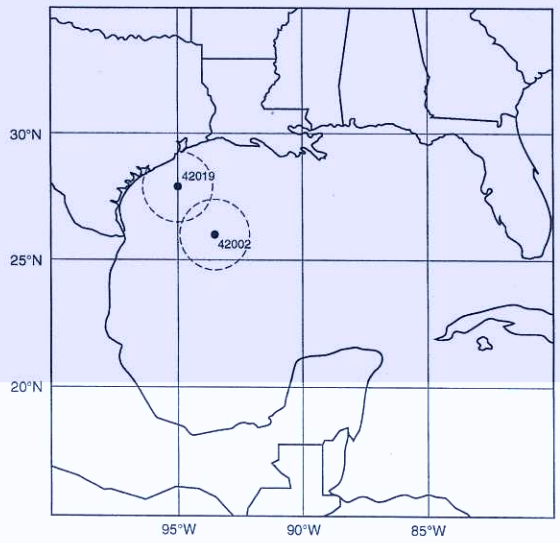

Fig. 1. The locations of NDBC buoys at stations 42019 (27.9°N, 95.0°W) and 42002 (25.9°N, 93.6°W) are shown together with co-located circles within which ship reports for search radii of 150 km were acquired (see text for details). The distance separating the buoys is 263 km.

moisture data are compared with reports from nearby ships and other fixed platforms. During the measurement period, a number of synoptic events occurred. We have taken this opportunity to examine the response of the Rotronic instrument to these events. Next, surface fluxes of heat and moisture are calculated from the buoy observations by using standard bulk parameterizations. Finally, we broaden the scope of this study somewhat by including additional calculations of selected wave parameters, again, using observations acquired from each of the buoys. In a companion study, Breaker et al. (1997) describe the sensor reliability and calibration procedures in greater detail, but do not include the applications given here.

2. Instrument description

2.1. Background

The Rotronic MP-100 humidity sensor has been under development since about 1980. The initial design was fragile and susceptible to contamination (Crane and Boole, 1988). Later versions of the instrument have proven to be more reliable. The Rotronic MP-100 is classified as a thin film capacitive polymer sensor (Crescenti et al., 1990). The operation of the instrument is based on the principle of capacitance change as the polymer which it employs absorbs and desorbs water vapor. A Gor-Tex filter, which covers the instrument transducer, allows water vapor (but not liquid water) to reach the sensor. Contaminants reduce the passage of water vapor through the filter which can lead to erroneous reports of saturation following high moisture events. As a result, the filter must be kept clean (Van der Meulen, 1988). Although the Rotronic MP-100 sensor has been used to measure moisture in the marine boundary layer, results in one case have indicated that early versions of the instrument may have suffered from hysteresis after periods of high relative humidity (Katsaros et al., 1994).

2.2. Deployment

Rotronic humidity sensors were installed on two NDBC buoys in the Gulf of Mexico located at 27.9°N, 95.0°W (station number 42019) and at 25.9°N, 93.6°W (station number 42002) (Fig. 1). The bottom depth at station 42019 is approximately 120 m, and at station 42002 it is approximately 3200 m. The sensor on station 42019 was installed on 4 May 1993; the sensor on station 42002 was installed on 4 June 1993. The platform at station 42019 is a 6-m NOMAD buoy with the Rotronic sensor mounted at a height of 3.9 m above the water line. The platform at station 42002 is a 10-m discus buoy with the Rotronic sensor mounted at 9.0 m above the water line.

2.3. Calibration

Fig. 2 shows pre- and postcalibration data for the instrument installed at station 42019. This sensor was calibrated on 27 January 1993 prior to its deployment on station 42019 and functioned normally until it was retrieved on 25 January 1994. When the sensor at station 42019 was recalibrated on 24 March 1994, there was a calibration shift of less than 2%. Most of this shift occurred at relative humidities of 70% or less. Finally, both the pre- and postcalibrations for station 42019 agreed with the reference values and also fell within the WMO accuracy standards (shown by the dashed lines in Fig. 2) which require accuracies of ±5% for relative humidities of

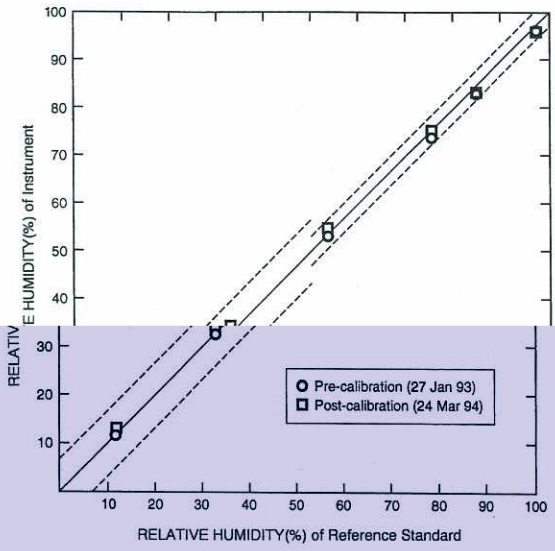

Fig. 2. Pre- and postcalibration data for the Rotronic humidity sensor installed on the buoy at station 42019 between 4 May and 25 January 1993 are shown. The dashed lines indicate the accuracy limits established by the WMO for humidity sensors. Both pre- and postcalibrations fall well within the specified limits.

Table 1
Reliability of Rotronic sensors deployed on various NDBC buoys

Year deployed	Sensors deployed	Sensors surviving > 6 months	Mean time between failures (months)
1989	13	4	4.5
1990	11	2	3.1
1991	15	7	5.0
1992–1994	10	6	6.5

up to 50%, and ±2% for relative humidities above 50% (World Meteorological Organization, 1983). The Rotronic sensor at station 42002 operated continuously until 7 February 1997 when the buoy power supply failed (~ 3.5 years).

2.4. Reliability

Since the Rotronic sensors were first installed on NDBC buoys along the West Coast, their reliability has steadily improved. Table 1 shows the number of instruments that survived more than 6 months, the number of sensors deployed, and the mean time between failures by year of deployment. The number of instruments that survived more than 6 months increased from two of 12 in 1990 to 6 of 10 between 1992 and 1994 due primarily to improvements in the cabling and calibration procedures. The mean time between failures for sensors deployed since 1991 is 8 months with one sensor lasting for more than 42 months. Table 2 examines the results above based on buoy hull type. Sensor survival on the small buoys is almost identical to that on the larger 10D buoys even though exposure of the sensor to salt spray obviously is greater on the 3D and the 6N buoys. This survival pattern has not changed with time and is significant because most of the new buoys that are being deployed by NDBC are either the 3D or the 6N hull types.

3. Data acquisition and analysis

3.1. Acquisition

The following environmental parameters were acquired from the buoys at stations 42019 and 42002 on an hourly basis for the period 5 June through 30 November 1993: barometric pressure, 8-min average wind speed and direction, air temperature, sea surface temperature, relative humidity, and one-dimensional wave spectra. From these measurements, the specific humidity was calculated (see Section 3.2 for details). The winds at station 42019 were acquired at an elevation of 4.9 m above the surface, while the winds at station 42002 were acquired at an elevation of 10.0 m above the surface. Sea surface temperature (SST) is measured through the hull of the buoy by a thermistor insulated from the interior hull environment at a depth of 1.0 m at station 42019 and 1.5 m at station 42002. The barometric pressure is measured at the water line (i.e. at an elevation of 0 m), while the air temperature is measured at a height of 3.7 m on station 42009 and 9.6 m on station 42002. Less than 0.5% of the data did not meet NDBC standards for quality control [1], or were missing. In these cases, previous values were either repeated or linear interpolation was used to fill in the missing data or to replace erroneous data in order to complete the time series for later Fourier analysis.

All variables from both buoys were adjusted to a standard reference height of 10 m by using the following procedures. First, barometric pressure at the buoys was converted from a height of 0 m to a height of 10 m using the hydrostatic equation. Next, the following equations were used to adjust the values of wind speed (U), air temperature (T), and specific humidity (q) from their observed heights to a height of 10 m (z_{10}) by using standard log profile relations and assuming near-neutral stability and negligible adiabatic effects in the surface layer (Panofski and Dutton, 1984):

$$(U_{10} - U_0)/U_* = \kappa^{-1} \ln(z_{10}/z_0)$$

$$(T_{10} - T_0)/T_* = \kappa^{-1} \ln(z_{10}/z_0)$$

$$(q_{10} - q_0)/q_* = \kappa^{-1} \ln(z_{10}/z_0)$$

where the subscript o refers to the observed height, U_* represents the surface friction velocity for wind

[1] Quality control of humidity data at NDBC includes automatic flagging of the data for which the relative humidity (RH) is < 0% or > 102%, and a time continuity check for which the change in RH must be ≤ 25% per hour. Temperature–dew point inversions are also flagged. Finally, all flags which are raised automatically are also checked manually (T. Mettlach, an oceanographer with Neptune Systems of Slidell, LA who conducted the field evaluations of the Rotronic sensor for NDBC, personal communication.).

Table 2
Survival of Rotronic sensors by hull type. Hull types are 3-m discus (3D) buoy, NOMAD (6N) buoy, and 10-m discus (10D) buoy. The Rotronic sensors are located at a height of 3.9 m on 3D and 6N buoys and at a height of 9.0 m on the 10D buoys

Year	3D and 6N buoys [a]				10D buoys			
	Total number	< 2 months	2–6 months	> 6 months	Total number	< 2 months	2–6 months	> 6 months
1989–1990	16	8	4	4	8	4	2	2
1991–1994	14	2	5	7	11	1	4	6

[a] These buoys have their wind, air temperature, and relative humidity instruments located at the same heights.

speed, T_* and q_* represent the corresponding values for temperature and moisture, and κ is von Karman's constant taken to be 0.4. To calculate U_*, T_*, and q_*, the following parameterization for the roughness length, z_0, was used:

$$z_0 = a\left(U_*^2/g\right)$$

where a is the Charnock constant taken to be 0.0185 (Wu, 1980), and g is the acceleration of gravity (9.8 m/s^2).

3.2. Moisture and flux calculations

Specific humidity at 10 m was calculated according to Gill (1982) as:

$$q_a = (0.62197 e_a)/(P - 0.378 e_a)$$

and the specific humidity at the ocean surface as:

$$q_w = (0.62197 e_w)/(P - 0.378 e_w)$$

assuming that the air is saturated at the surface. q_a and q_w are expressed in grams of water vapor per kilogram of moist air. e_a represents the vapor pressure of air (hPa), e_w the vapor pressure (hPa) at the temperature of the ocean surface, and P is the barometric pressure (hPa) at sea level.

e_a is, in turn, calculated according to:

$$e_a = \mathrm{RH}\, e_s/100.0$$

where RH is the relative humidity in percent, and e_s is the saturation vapor pressure of the air at 10 m (List, 1966). e_w is computed from:

$$e_w = K \times 10^{\upsilon}\left[1.0 + 1.0 \times 10^{-6} P\left(4.5 + 0.0006 T_0^2\right)\right]$$

where T_0 is the sea surface temperature (°C), υ is computed from:

$$\upsilon = (0.7859 + 0.03477 T_0)/(1.0 + 0.00412 T_0)$$

and K is a reduction factor for saturation vapor pressure over seawater. At a salinity of 35 ppt (assumed here), K is taken to be 0.98 (Kraus and Businger, 1994).

Surface fluxes of sensible and latent heat were calculated from the appropriate buoy observations and the specific humidities following standard bulk parameterizations (e.g. Kraus and Businger, 1994), expressed as:

$$Q_S = -\rho_a C_p C_Q (T_{10} - T_0) U_{10}$$

for the sensible heat flux (Q_S in W/m^2), where ρ_a and C_p are the density (1.225 kg/m^3) and the specific heat at constant pressure (1004.0 J/kg/°K) for air, respectively, and C_Q is the bulk transfer coefficient for sensible heat. The latent heat flux (Q_E in W/m^2) is:

$$Q_E = -\rho_a C_E L_v (q_{10} - q_w) U_{10}$$

where L_v is the latent heat of vaporization ($2.5008 \times 10^6 - 2300.0 T_0$ (°K)), and C_E is the bulk transfer coefficient for water vapor. For near-neutral conditions (which have been assumed throughout), C_Q and C_E are approximately equal and have a value of about 1.2×10^{-3} (Kraus and Businger, 1994), the value used here. It is important to note that the inherent uncertainty in these formulations is high (at least several tens of W/m^2 according to Blanc, 1985). As a result, we have also calculated these heat fluxes by using slightly different parameterizations; however, the results were generally similar to those presented here.

3.3. Wave calculations

Vertical acceleration at the buoys is measured every 0.67 s for a period of 20 min each hour. The acceleration records are integrated and Fourier-trans-

formed to obtain the wave energy density spectrum. Wave energy density spectra $F(f)$ as a function of the frequency, f, were calculated with a resolution of 0.01 Hz for frequency ranges of 0.03–0.40 and 0.03–0.50 Hz at station 42002 and 42019, respectively. From these spectra, three additional wave parameters have been calculated. The first is the significant wave height H_s, defined as:

$$H_s = 4.0\sqrt{\int_0^\infty F(f)\mathrm{d}f}$$

which provides a direct measure of the wave activity.

Since we are primarily interested in the wave parameters which may be related to the exchange of moisture between the ocean and the lower atmosphere, the process of wave breaking is clearly important. However, wave breaking is a discrete process in time, which is not directly captured in the above frequency–domain representation of the wave observations. The intensity of wave breaking, however, appears to be related to the development stage of the wave field, which also governs wave-induced surface roughness. The latter parameter is thus also most likely linked to the surface moisture flux and is a parameter which can be estimated directly from the wave energy density spectrum. The overall development stage of the wave field can be described with the inverse wave age:

$$\epsilon = U/C$$

where C is the phase velocity corresponding to the peak frequency of the spectrum, and U is the wind speed. The peak frequency, f_p, is estimated from the maximum discrete spectral estimates and its neighboring values by fitting a second-order polynomial to the spectra. From this frequency, C is determined using the standard dispersion relation for wave speed in water of arbitrary depth. $\epsilon \approx 1$ corresponds to a fully developed wind sea, i.e. a wind sea in equilibrium with the local wind sea, $\epsilon > 1$ corresponds to growing wind waves and $\epsilon < 1$ corresponds to swell. The wave-induced contribution to the surface stress is important for young waves only ($\epsilon > 1$).

Because the wave-induced roughness is primarily related to high-frequency wave energy, another parameter of interest is the non-dimensional energy of the high-frequency flank of the spectrum α, also known as the 'Phillips' constant (Phillips, 1958), where:

$$\alpha = (2\pi)^4/g^2(f_h - f_l)\int_{f_l}^{f_h} F(f)f^5\mathrm{d}f$$

and:

$$f_l = 1.5^* \max(f_p, f_{PM})$$

$$f_h = \max(2.5^* f_p, 2.5^* f_{PM}, f_{max})$$

and where f_{PM} is the Pierson–Moskowitz frequency (Pierson and Moskowitz, 1964) for which $\epsilon = 1$ at a given wind speed, and f_{max} is the highest spectral frequency observed. α is a measure of the small-scale roughness of the ocean surface, and therefore of the wave-induced surface stress. For a fully developed sea, $\alpha \approx 0.01$, and the wave-induced stress will again be small. For larger α, active wave growth occurs, and waves will contribute significantly to the surface stress. For smaller α, the contribution of waves to the surface stress is small. In such cases, most of the wave energy can be attributed to swell. The limited range of frequencies for which the wave spectra are observed, however, makes it impossible to evaluate α for low wind speeds and/or low wave heights. This parameter has only been evaluated for cases where the integral encompasses at least four discrete spectral densities. Note that α is still an indirect measure of the surface roughness. The actual roughness is primarily related to near-capillary waves which are well outside the range of the present wave observations. Furthermore, ϵ and α generally behave similarly, since they can be considered as large-scale (ϵ) or small-scale (α) estimates of the wave-induced surface roughness.

4. Results

4.1. Validation

To provide a measure of validation for the observations of moisture acquired from the buoy-mounted Rotronic humidity sensors, we have made comparisons of buoy data with measurements of boundary layer moisture acquired from selected ships and fixed platforms (primarily oil rigs) in the surrounding area. The majority of ship reports came from two NOAA

research vessels (NOAA Ships OREGON II and CHAPMAN) which were at sea in the Gulf of Mexico during the study period. Each vessel was equipped with wet and dry bulb thermometers and used standard WMO data collection and reporting procedures.

All of the reported moisture values obtained from the ships and fixed platforms were converted to specific humidities for direct comparison with the calculated specific humidities from the buoys. Since the observing heights of the humidity measurements aboard the ships were not known, no adjustments to a standard reference height were made for either the ship reports or the buoy measurements. The observations from each source were matched to within 1 h in time and over a range of search radii from each of the buoys (we refer to these matched pairs of ship/platform and buoy observations as 'matchups' hereafter). The search radii were increased in 25-km steps from 50 out to 300 km for each buoy. Fig. 1 shows matchup circles for each buoy with search radii of 150 km. Biases, RMS differences, and correlations between the buoy and the ship reports are given in Table 3 for search radii of 50–300 km (in 50 km steps). The RMS differences are slightly higher and the correlations lower for the sensor on buoy 42002. In all cases, where sample sizes exceeded 33, the correlation coefficients between the buoy and the ship reports exceeded 0.70 and were statistically significant at the 99% level of confidence. Although the buoy moistures on average tend to be slightly higher than the ship moistures for the sensor on buoy 42019 (indicated by the positive biases), the opposite is true for the sensor on buoy 42002. The differences between the buoy and the ship reports are of the same order as the height adjustments that could have been applied, if the observing heights had been available. Thus, no definitive statements can be made concerning their significance. Additional validation studies are contained in Breaker et al. (1997).

Table 3
Comparisons of specific humidities at NDBC buoys 42019 and 42002 with those computed from nearby ships and fixed platform observations at various radii from each buoy

Range (km)	Sample size	Bias (g/kg)	RMS (g/kg)	Correlation coefficient
Station 42019				
50	49	0.43	1.33	0.932
100	170	0.59	1.66	0.893
150	326	0.89	2.00	0.868
200	472	0.81	2.04	0.867
250	622	0.73	2.00	0.867
300	733	0.67	2.02	0.852
Station 42002				
50	8	−1.67	2.20	0.780
100	33	−1.32	2.23	0.550
150	101	−1.46	2.76	0.712
200	166	−0.98	2.37	0.728
250	333	−0.84	2.14	0.786
300	580	−0.71	2.24	0.780

Katsaros et al. (1994) reported on field tests conducted in 1986 on a number of humidity sensors including the Rotronic MP-100 instrument. Hysteresis was found to occur following high-moisture events for the Rotronic MP-100 instrument. The greatest differences between the Rotronic sensor and a reference psychrometer occurred at relative humidities less than 70%, particularly after periods of high relative humidity. The Rotronic sensor apparently required time to dry out after periods of high moisture. Finally, a bias of 8% between the Rotronic MP-100 and a reference psychrometer was not due simply to a calibration error, but was attributed, in part, to hysteresis by the sensor.

To address the problem raised by Kataros et al., we first looked for periods of high relative humidity in our data. Unfortunately, very few periods of identifiable rain occurred during the study period, and those periods which could be identified did not coincide precisely with any of our ship reports. Thus we could not adequately address the hysteresis problem raised by Katsaros et al. However, the observations presented by Katsaros et al. were acquired in 1986, and, according to the manufacturer, several improvements were made to the instrument subsequent to this period including: (1) a change to the polymer to improve its ability to resist a variety of contaminants; and (2) the filter was changed from steel to Gor-Tex to prevent penetration of salt particles (F. Fetkowitz, an instrument engineer and US field representative for the Rotronic Instruments Corp., personal communication). As a result, the hysteresis problem identified by Katsaros et al. was most likely solved by the time the present evaluation was initiated. Also, based on the results of Visscher

and Schurer (1985), Muller and Beekman (1987), and Hundermark (1989), hysteresis problems were not previously found with the Rotronic MP-100 instrument.

4.2. Temporal variability of environmental parameters

Time series of sea-level pressure, wind speed, wind direction, sea surface temperature, air temperature, specific humidity (at 0 and 10 m) and significant wave height are shown in Fig. 3 (station 42019) and Fig. 4 (station 42002). Specific humidity at the surface follows sea surface temperature, upon which it is primarily based, but does not respond strongly to the atmospheric conditions above, at least on synoptic and shorter time scales. As a result, the pattern of variability which occurs at the surface is quite different from that which occurs at 10 m. Surface specific humidity in most cases exceeds that at 10 m. However, during brief periods in October and November, the specific humidity at 10 m does exceed that at the surface (for buoy 42019 only). In these cases, the air passing over the buoys has been modified significantly through the exchange of heat and moisture with the underlying ocean.

During the months of June through August 1993, little synoptic variability occurred. However, during mid-June, tropical storm Arlene entered the Gulf of Mexico and affected specific humidity at both buoy locations. Beginning in mid-September, synoptic variability increased significantly. Most of the synoptic events that occurred between September and November were associated with the so-called 'return flow cycle', a sequence of events that leads to the initiation and termination of return flow over the Gulf of Mexico (Crisp and Lewis, 1992). Breaker et al. (1997) describe one such event that took place between October 30 and November 3, 1993, in detail. This variability is primarily frontal in nature and has been described by DiMego et al. (1976) and Henry (1979).

On 26 September, specific humidity dropped suddenly at both buoys due to the first significant return flow event of the fall season. This system was composed of two fronts, a weaker front closely followed by a front which was more intense. On 27 September, the first front weakened significantly, while the second front passed the buoy at station 42019 as it moved toward station 42002. Later on the 27th, the dominant front passed station 42002 with increasing wind speeds and falling air and dew point temperatures [2]. Dew point temperatures dropped by over 10°C at station 42019 and by ~ 5°C at station 42002, indicating that the air mass behind the front was not only cold, but relatively dry. The impact of this frontal passage was clearly greater at station 42019 than it was at station 42002 for all buoy parameters. By 30 September, the impact of the return flow event had practically disappeared at both buoy locations.

Starting on 21 October, a series of cold fronts began dropping down into the Gulf of Mexico and continued with some regularity through the end of November. Between 21 and 29 October, two cold fronts entered the Gulf from the NW and, within a day or two, each system had weakened significantly. On 30 October, a rapidly moving, intense frontal system entered the Gulf from the north. The air mass behind this front was extremely cold and dry. Dew point temperatures at station 42019 dropped to a low of 3.9°C and at station 42002 they reached 6.7°C as the center of high pressure behind the front continued to move south and into the area where the buoys were located. It was nearly 5 days before the return flow event subsided. On 6 November, another cold front dropped down into the northern Gulf close behind the previous front. Although this frontal system was intense, it was slightly weaker than the previous system.

Between 9 and 11 November, a small high-pressure system dropped down over the northern Gulf bringing slightly cooler and drier continental air with it, unlike the previous events, which were primarily frontal in nature. Between 17 and 30 November, three more cold fronts dropped down into the Gulf of Mexico causing air and dew-point temperatures to drop significantly at the two buoy locations.

In summary, both DiMego et al. and Henry show a minimum of frontal activity from June through

[2] Although dew point temperatures are not shown, they were calculated from the relative humidities obtained from the buoys and were available to the authors as were the dew points displayed on the NCEP final analyses which were used for this discussion.

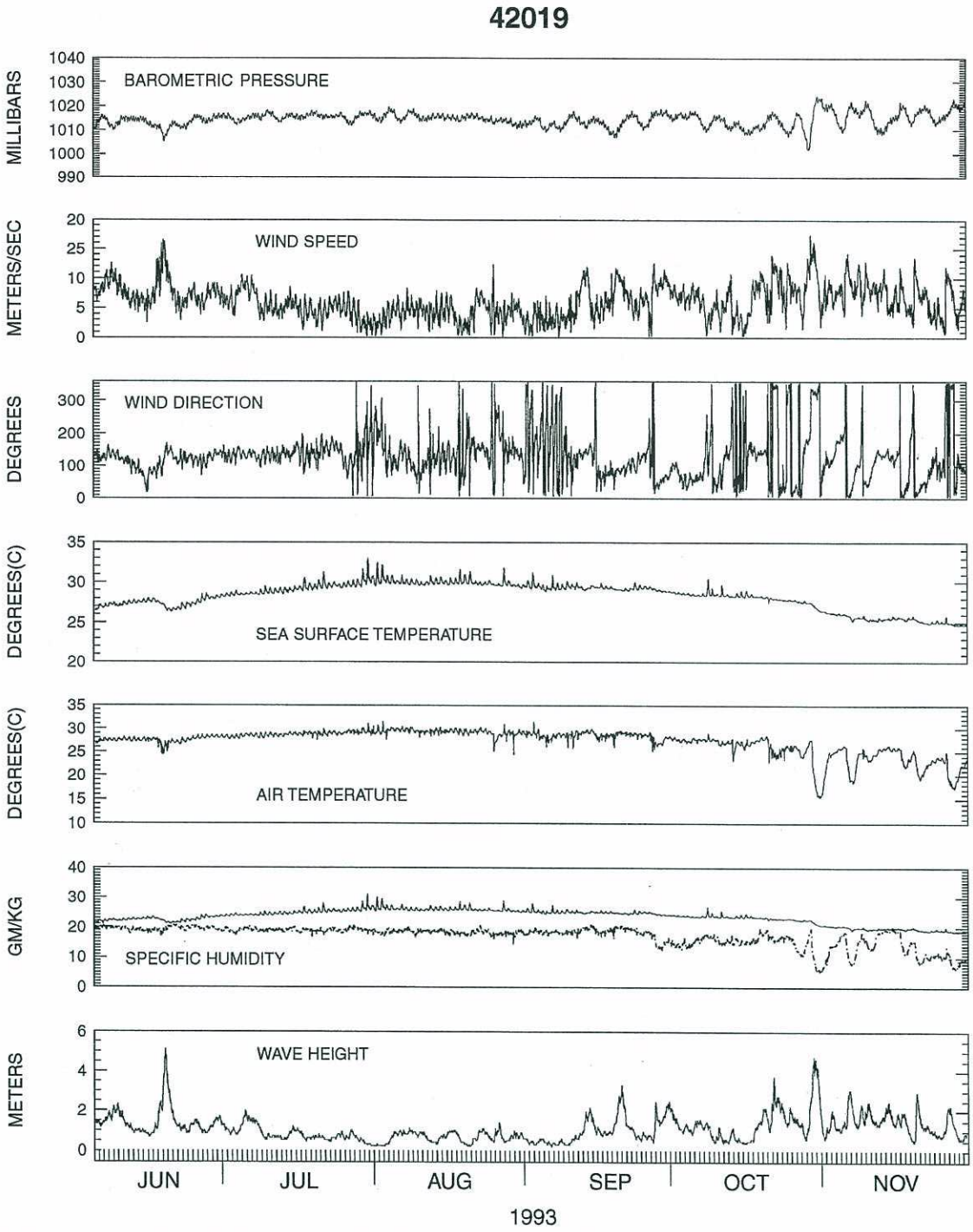

Fig. 3. Time series of hourly sea-level pressure, wind speed, wind direction, sea surface temperature, air temperature, specific humidity, and significant wave height are shown for the period 5 June through 30 November 1993, for the buoy at station 42019.

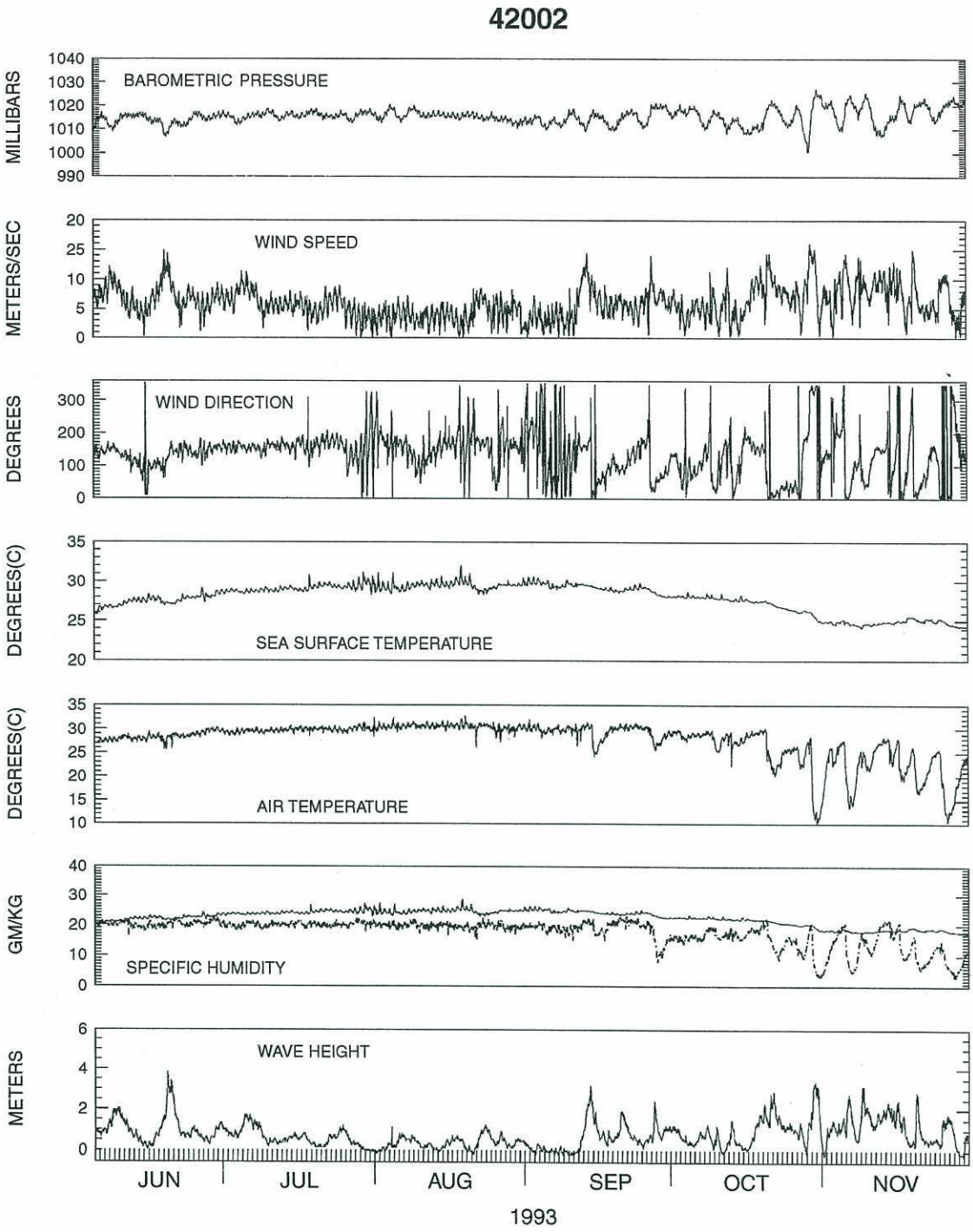

Fig. 4. Same as Fig. 3, except for the buoy at station 42002.

August, a maximum of frontal activity from November through March, and a short, dramatic increase in activity during September and October. According to Henry, fronts can enter the Gulf of Mexico in any month. In our case, no fronts entered the Gulf during June, July, or August 1993, but during September, October, and November 1993, 2, 3, and 4 fronts, respectively, entered the Gulf. Because the weaker fronts dissipated before reaching station 42002, more synoptic activity occurred at station 42019 than at station 42002 from September through November. These events produced strong and well-defined signatures in the moisture-related observations, emphasizing the importance of these data in characterizing synoptic-scale variability in the near-surface marine environment.

Cross-correlation analyses were performed for the two buoy time series of specific humidity, wind speed, barometric pressure, air temperature, sea surface temperature, and significant wave height. The maximum cross-correlations and the corresponding lags are presented in Table 4. The correlation coefficients consistently exceed 0.9, except for wind speed and wave height where local (wind speed) or cumulative (wave height) effects become important. Of particular interest are the lag relationships between the time series for each parameter. Of the atmospheric parameters, air temperature and specific humidity both attain their maximum correlations at lags of −6 and −7 h, respectively, whereas the other parameters are maximally correlated at, or near, zero lag. Lags of −6 or −7 h indicate that coherent sources of variation occur at station 42019 prior to their occurrence at station 42002, consistent with

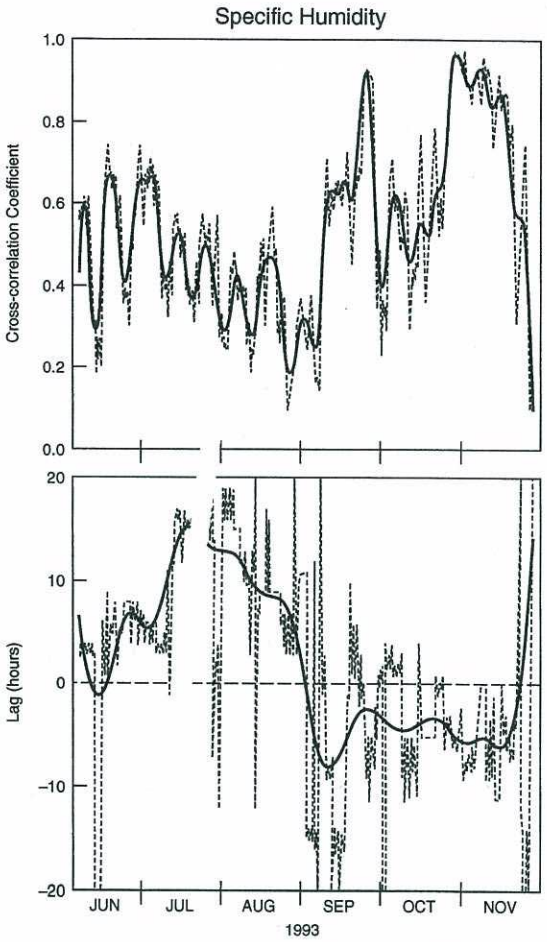

Fig. 5. Cross-correlations for specific humidity between the buoys at stations 42019 and 42002 at 10 m for successive 7-day segments of the time series at 1-h time increments. The maximum cross-correlations are plotted in the upper panel and the corresponding lags (h) in the lower panel. The dashed curves represent the original values and the solid curves, the results after smoothing. See the text for the interpretation of this figure.

Table 4
Cross-correlation statistics for the entire series of hourly values for the environmental parameters included below from 0000 UTC, 5 June to 2300 UTC 30 November 1993

Environmental parameter	Cross-correlation	Lag (h)[a]
Specific humidity	0.911	−7
Wind speed	0.678	−1
Barometric pressure	0.939	0
Air temperature	0.943	−6
Sea surface temperature	0.910	0
Significant wave height	0.820	−5

[a] Negative sign indicates that the series at station 42019 leads the series at station 42002.

atmospheric disturbances which propagate from the NW with speeds on the order of 10–15 m/s. Based on a maximum cross-correlation of 0.91, a separation distance of 263 km between the buoys, and an exponential decay law, the *e*-folding distance for specific humidity is ~ 800 km, indicating that variations in moisture are spatially coherent over relatively large distances in the northern Gulf of Mexico. With respect to wave height, a lag of −5 h was observed, which indicates that the prevailing direc-

tion of propagation for surface gravity waves in the northwestern Gulf of Mexico lies roughly between the southwest and northeast quadrants.

Successive cross-correlations for specific humidity were also calculated for 7-day (168-h) periods, stepping through the data hour-by-hour. The results are displayed in Fig. 5, where both the maximum cross-correlations (upper panel) and the corresponding lags (lower panel) are shown. The maximum correlations increase abruptly around 7 September, and the lags change from mostly positive to essentially negative at this time, indicating that events prior to the first week in September generally arrived at station 42002 before they arrived at station 42019 and conversely thereafter. These changes in correlation structure for specific humidity are significant and reflect a seasonal change in synoptic weather conditions in the northern Gulf of Mexico. In particular, they imply that the prevailing patterns became more coherent and tended to enter the buoy domain from the North rather than from the South after the first week in September, in agreement with the results of DiMego et al. (1976) and Henry (1979).

4.3. Spectral calculations

The time series of wave height, wind speed, specific humidity, air temperature, SST, and barometric pressure have also been subjected to spectral analysis in order to further explore the character of the variability for the various buoy parameters. Prior to the spectral computations, each time series was

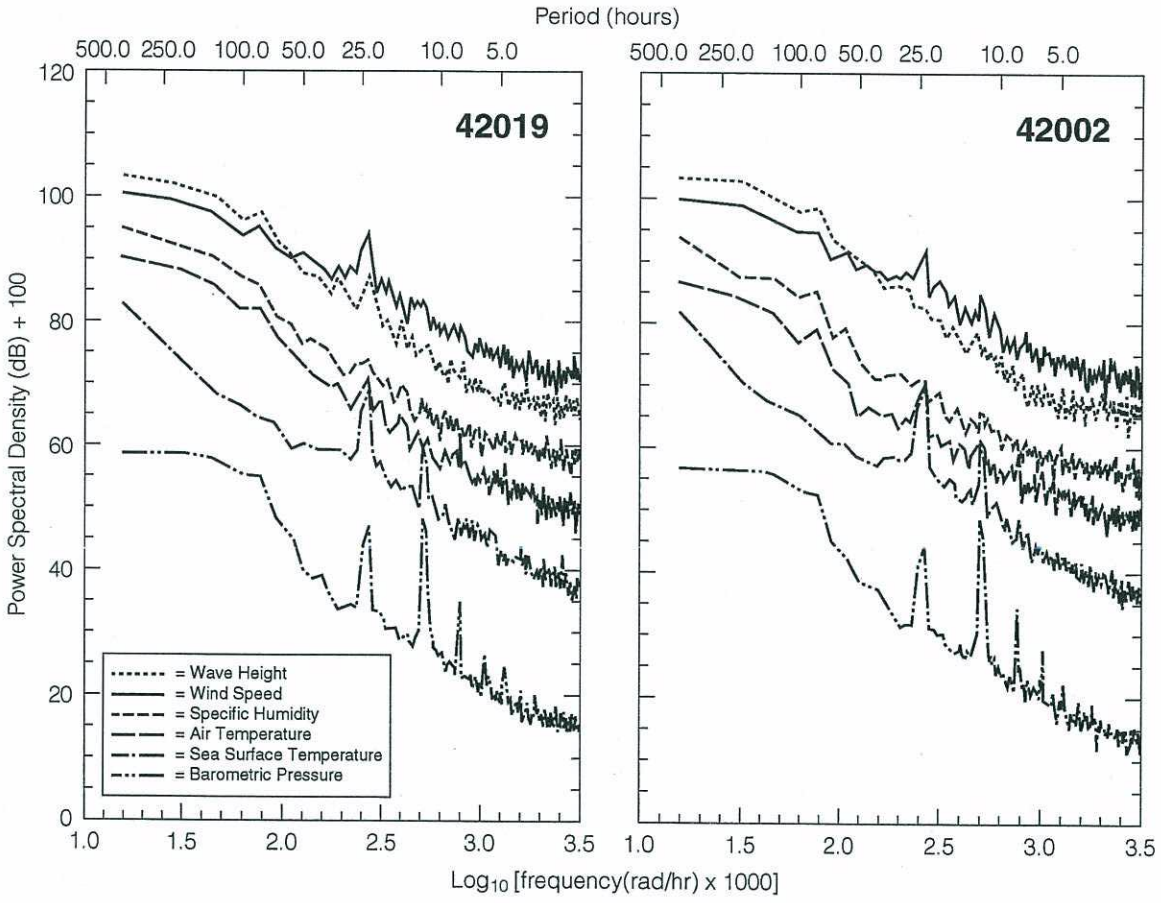

Fig. 6. Autospectra for each of the buoy parameters for stations 42019 (left-hand panel) and 42002 (right-hand panel). Each series was divided by its mean and then centered before the spectra were calculated. The spectra correspond to smoothed periodograms obtained using a Fast Fourier Transform and are plotted in log–log coordinates.

normalized with respect to its mean; the resulting non-dimensional series were then centered. The spectral computations were performed by first calculating raw spectral estimates using a Fast Fourier Transform and then smoothing with a Parzen spectral window (IMSL, 1982). Fig. 6 shows the autospectra

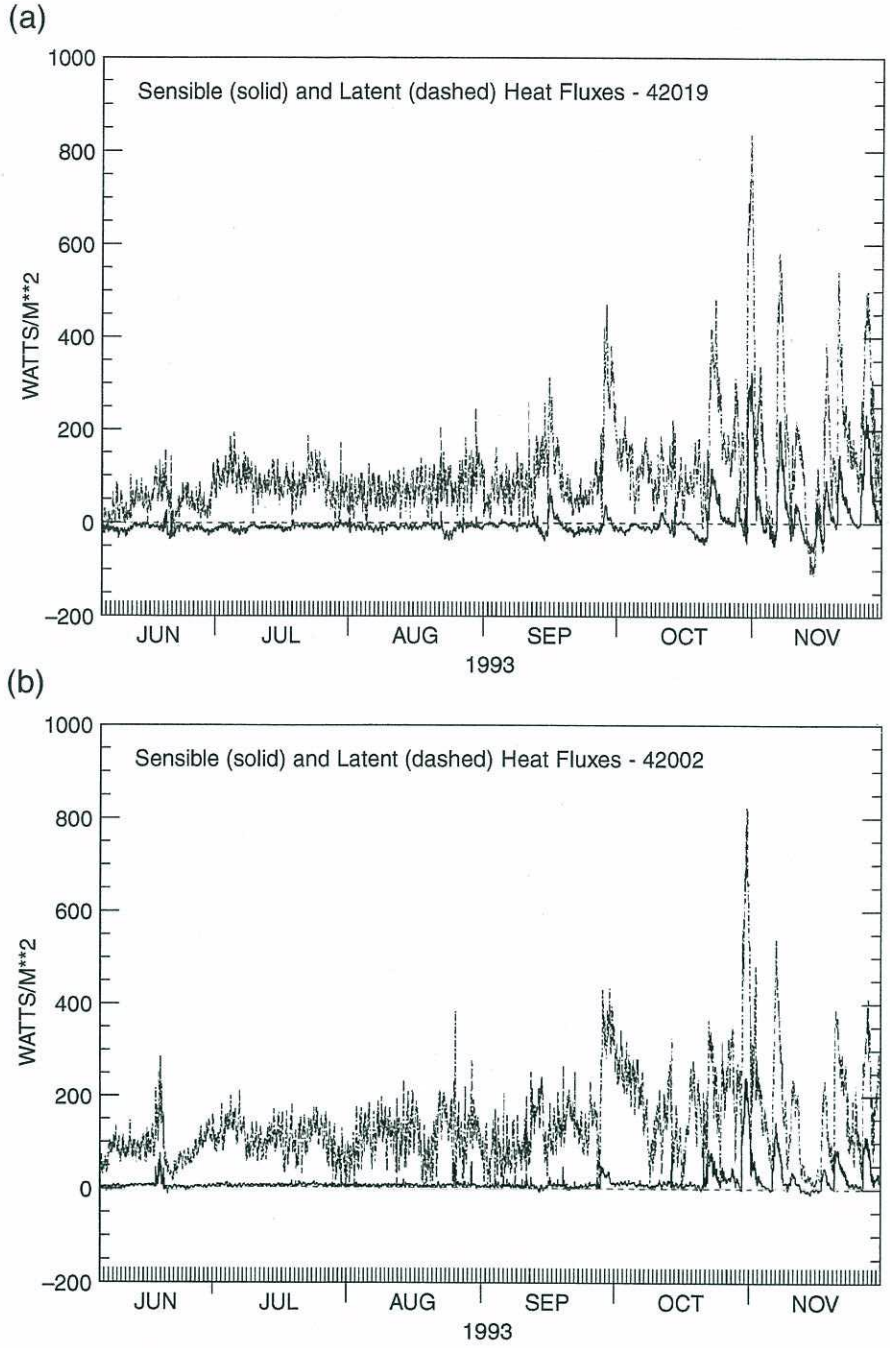

Fig. 7. Hourly time series of latent (upper) and sensible (lower) heat fluxes for the period 5 June through 30 November 1993 are plotted for the buoy at station 42019 in the upper panel and also for the buoy at station 42002 in the lower panel.

for each of the parameters plotted together for station 42019 (left-hand panel) and station 42002 (right-hand panel).

All of the autospectra display similar negative slopes which are characteristic of most geophysical processes (the so-called 'red noise' spectrum). Obvious spectral peaks occur at periods of 12 and 24 h for barometric pressure, SST and air temperature (but no obvious peak in air temperature at 12 h for station 42019), and lesser peaks at 24 h for wind speed and wave height. Weaker peaks can be detected at a period of ~80 h for most parameters, and most likely correspond to the passage of synoptic scale events of atmospheric origin. At both buoy locations, the autospectra for wind speed and wave height are similar (they actually cross at 'x' = ~2.1 (50 h) in each case), reflecting the close relationship that exists between the wind forcing and the wave response.

4.4. Surface heat fluxes

The calculated latent and sensible heat fluxes are plotted together for buoy stations 42019 (upper panel) and 42002 (lower panel) in Fig. 7. Selected summary statistics for the latent and sensible heat fluxes are given in Table 5 and are in close agreement with those contained in NOAA Atlas NESDIS 8 (da Silva et al., 1994). As expected, the latent heat fluxes far exceed the sensible heat fluxes in most cases for both buoys. The latent heat fluxes were almost always positive at both buoys; in contrast, the sensible heat fluxes were positive almost 90% of the time at station 42002; whereas, they were only positive approximately 22% of the time at station 42019, most likely reflecting the influence of lower SSTs in the nearshore region during the fall and the close proximity to land. The peak values for both fluxes correspond closely with the major synoptic events which occur between September and November. Upon closer inspection, the flux maxima tend to coincide with the arrival or onset of these events rather than during the subsequent periods of recovery, consistent with the occurrence of the largest near-surface vertical gradients of temperature and moisture, and the expected response of the marine boundary layer. Overall, the heat transfer, which is dominated by the synoptic events which take place after mid-September, is primarily from the ocean to the atmosphere.

Table 5
Selected summary statistics for the latent and sensible heat fluxes

	Station 42019	Station 42002
Latent heat flux (LHF)		
Maximum (W/m^2)	864.7	841.9
Minimum (W/m^2)	−115.2	2.4
Mean (W/m^2)	109.6	174.3
Time negative (%)[a]	3.0	0.0
Sensible heat flux (SHF)		
Maximum (W/m^2)	329.4	243.9
Minimum (W/m^2)	−63.4	−14.9
Mean (W/m^2)	2.3	11.7
Time negative (%)[a]	77.6	11.0

[a] Heat transfer from the atmosphere to the ocean.

4.5. Surface gravity waves

Certain physical processes associated with surface gravity waves are responsible for introducing moisture into the marine boundary layer. Wu (1974) has estimated that as much water enters the atmospheric surface layer through the evaporation of water droplets (from breaking waves, for example) as that which is contributed through direct evaporation from the ocean surface itself, for a wind speed of 15 ms^{-1} at 10 m. Fairall et al. (1990) suggest that latent heat fluxes are not only related to wind speed and air–sea temperature difference, but also, at least weakly, to the surface roughness, a wave-related parameter. Thus, we examined the time series of significant wave height and several related parameters in greater detail.

Fig. 8 (station 42019) and Fig. 9 (station 42002) show significant wave height, inverse wave age and the Phillips constant, and latent heat flux for both buoys for the entire period. As with the other buoy parameters, several distinct weather regimes can be identified in the time histories of the various wave parameters. The first 4 months through mid-September generally show quiescent wave conditions, briefly

Fig. 8. Time series of significant wave height, wave age (inverse), wave roughness (α), and latent heat flux for the buoy at station 42019 for the period 5 June through 30 November 1993.

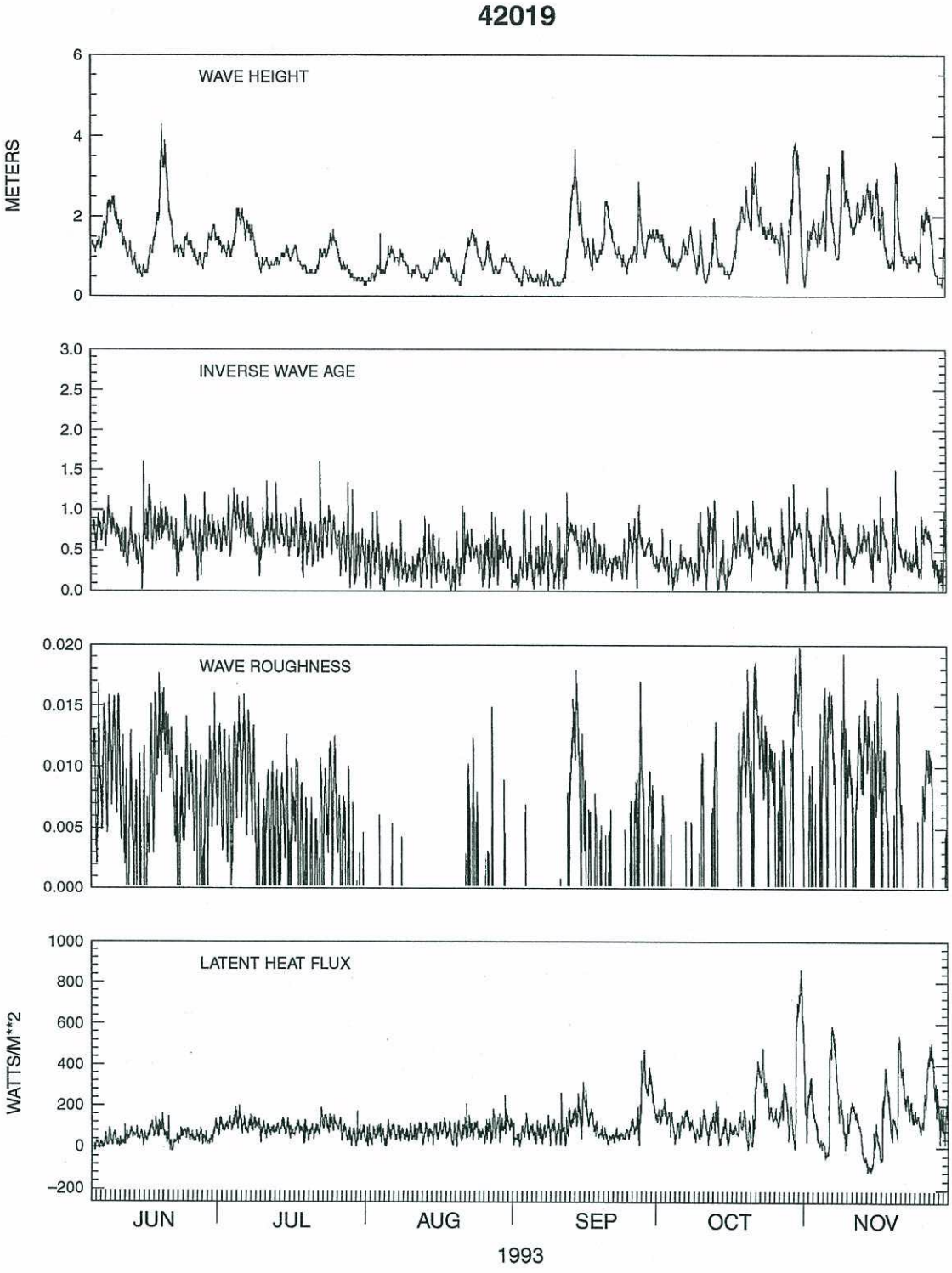
42019
WAVE HEIGHT
METERS
6
4
2
0
INVERSE WAVE AGE
3.0
2.5
2.0
1.5
1.0
0.5
0.0
WAVE ROUGHNESS
0.020
0.015
0.010
0.005
0.000
LATENT HEAT FLUX
WATTS/M**2
1000
800
600
400
200
0
−200
JUN
JUL
AUG
SEP
OCT
NOV
1993

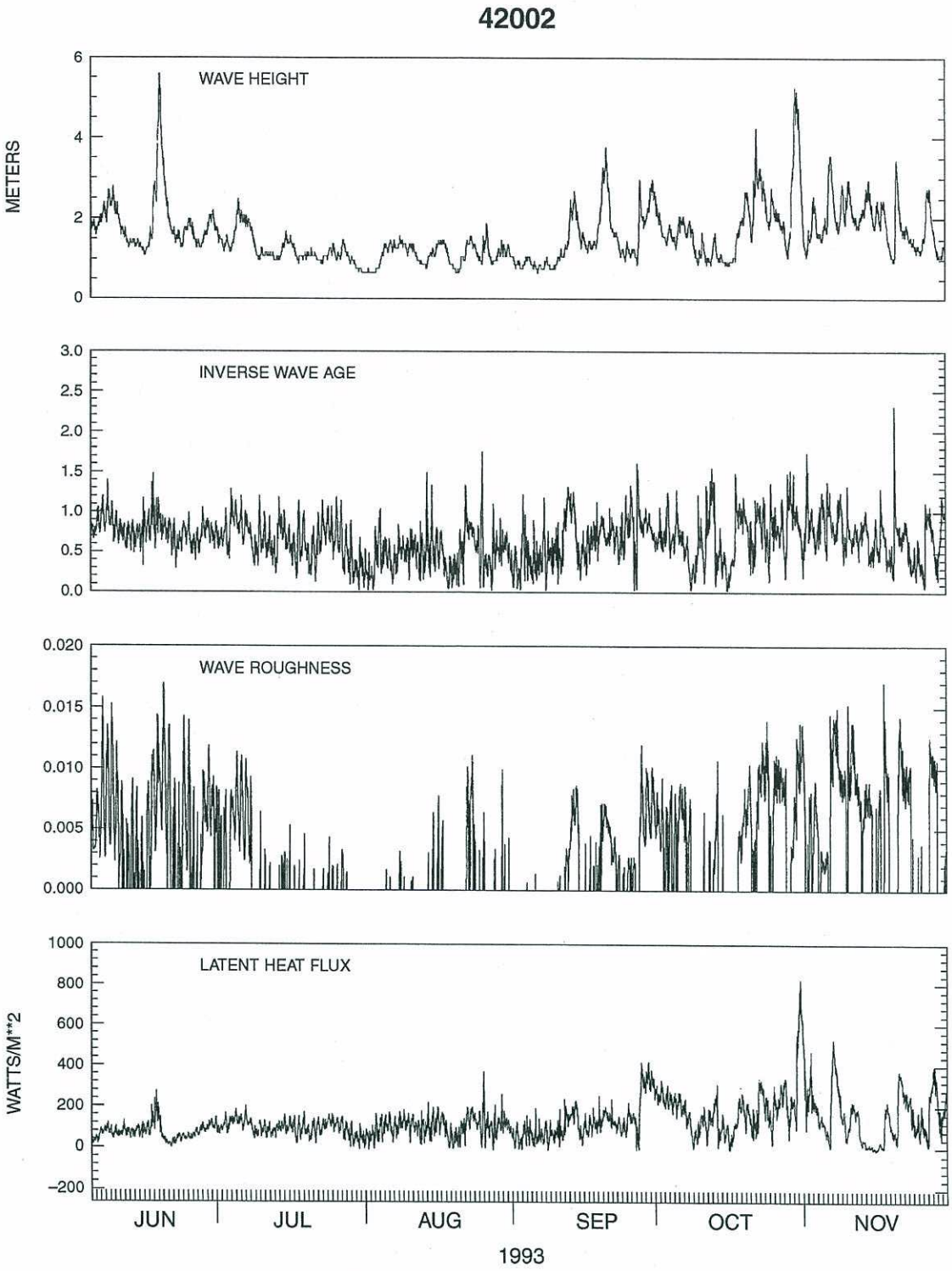

Fig. 9. Same as Fig. 8 except for the buoy at station 42002.

interrupted by the passage of tropical storm Arlene from 17 to 21 June. The wave energy during this period consists primarily of swell, since the inverse wave age is consistently < 1. The wind speed (Figs. 3 and 4) shows a well-defined diurnal cycle, which may be related to diurnal changes in the stability of the marine boundary layer. The significant wave height shows a much smaller daily modulation since the total wave energy tends to be concentrated at the relatively low frequencies. The time scale of adjustment of waves to winds at these frequencies is relatively large, thus damping out rapid modulations of the wind speed. The inverse wave age shows a daily oscillation similar to that of the wind speed from which it is calculated. This indicates that the peak frequency, like the significant wave height, is rather insensitive to the daily wind speed modulations. In contrast, high-frequency wave energy has a much smaller time scale in responding to changes in the wind field, and hence is expected to show a much stronger response to the daily modulation of the wind. α does, in fact, show a large modulation, which lags the wind speed modulation by approximately 1–2 h. Due to the discontinuous nature of α, this lag could not be calculated objectively, but was instead estimated by inspection. The modulation of α suggests that the surface roughness also has a large daily modulation. Because surface roughness is primarily related to waves of shorter period than those which are incorporated in α and because such waves have an even smaller time scale of response to wind changes, the surface stress is expected to show a smaller time lag (if at all) with respect to wind speed than α.

As discussed earlier, the period from mid-September through the end of November shows a sequence of synoptic weather systems moving through the northern Gulf of Mexico. Particularly after mid-October at the offshore buoy (station 42002), the diurnal cycle in all buoy parameters either disappears, or is lost in the prevailing synoptic variability. At the nearshore buoy (station 42019), however, the diurnal cycle is still detectable. Several of the systems passing through the region (particularly at station 42019) produce young wind seas with ϵ significantly larger than 1 and α significantly larger than 0.01, for which wave-induced surface roughness and wave breaking are expected to be significant. The events with the most pronounced wave-induced roughness coincide with the most pronounced heat flux events. Furthermore, all latent heat flux (LHF) events coincide with distinct wave events.

To investigate the co-occurrence of active wave growth and LHF events further, LHF is plotted as a function of α in Fig. 10. To avoid the confounding effects of the large diurnal oscillations in α, average values for each day are presented. To ensure reasonable coverage of the daily cycle, a minimum of 18 observations of α per day was averaged. Fig. 8 indicates that the most extreme LHF events do, in fact, correspond to active wave growth conditions ($\alpha > 0.01$), at station 42019, in particular. A careful comparison of the α-values from the two buoy loca-

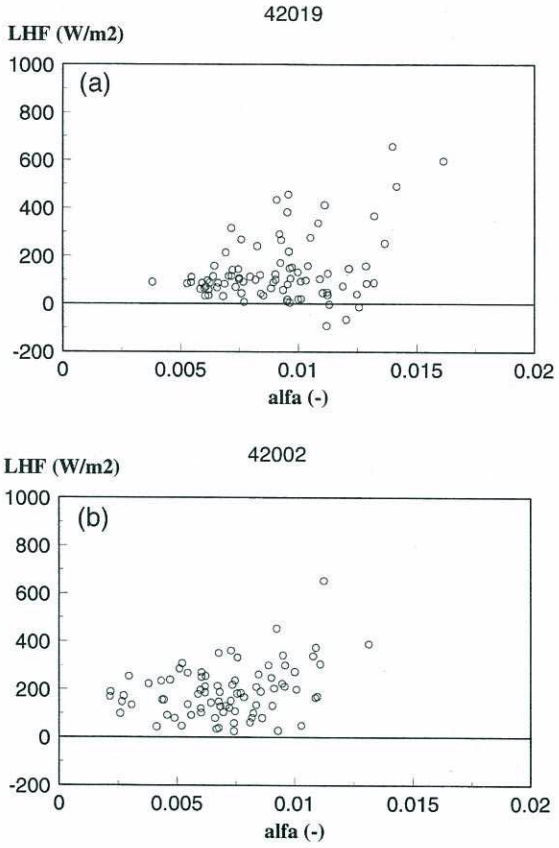

Fig. 10. Latent heat flux (W/m^2) versus surface wave roughness (α) for stations 42019 (a) and 42002 (b). The data were averaged daily before plotting reducing the number of points from 4296 to 179. See text for additional details concerning the data processing and the interpretation.

tions reveals that α is generally based on data near the limits of the frequency range that can be observed with the platforms considered. Systematic differences between the platforms might, therefore, be related to differences in the transfer functions for the different hull types (6-m NOMAD at station 42019 vs. 10-m discus at station 42002). Nevertheless, extreme LHF events clearly coincide with conditions of increased surface roughness due to active wave growth. With the present observations, however, we cannot identify any causal or functional relation between the two, but the co-occurrence of the heat flux events and the actively growing wind seas is consistent with the production of spray and bubbles through the process of wave breaking.

5. Summary and conclusions

The overall reliability of the Rotronic MP-100 humidity sensors which have been deployed on various NDBC buoys has improved significantly since 1989 when they were first considered for possible long-term deployment on fixed platforms at sea.

Over the approximate 6-month period that the Rotronic sensor installed on the buoy at station 42019 was deployed, its calibration remained within the accuracy limits set by the WMO. The Rotronic sensor installed on the buoy at station 42002 operated continuously from its deployment in June 1993 to buoy failure in February 1997 ($\sim$ 3.5 years).

According to Katsaros et al. (1994), an earlier version of the Rotronic sensor experienced hysteresis following periods of high moisture. Our data did not permit us to examine this question in detail due to the lack of precipitation during the period of observation. However, problems associated with hysteresis for the Rotronic sensor have not been reported elsewhere, which may be due to improvements that were made by the manufacturer subsequent to the observations of Katsaros et al.

Time series of specific humidity at a height of 10 m revealed three primary scales of variability: meso ($\sim$ h), synoptic ($\sim$ days), and seasonal ($\sim$ months). During the 6-month period of this study, most of the synoptic-scale variability occurred after the first week in September and was due to the arrival of frontal systems containing cold, dry air that dropped down into the Gulf of Mexico from the continental US. One exception occurred in June (1993) when tropical storm Arlene moved NNW across the Gulf strongly influencing the moisture field in the vicinity of the buoys. Overall, the moisture-related parameters acquired at the buoys (specific humidity, in particular) were highly sensitive to the various synoptic events and the seasonal variability that took place in the marine boundary layer during the period of this study.

A cross-correlation analysis between the buoys (for a separation distance of 263 km) for specific humidity and the other buoy parameters indicated that: (1) all parameters were highly correlated (> 0.9) except for wind speed and wave height; (2) the *e*-folding correlation distance for specific humidity was at least 800 km; and (3) specific humidity and air temperature both served as tracers of the motion associated with propagating atmospheric disturbances. A more detailed cross-correlation analysis of the specific humidity time series revealed a major change in correlation structure that occurred during the first week in September, indicating that weather patterns became more coherent and tended to enter the northern Gulf of Mexico from the North rather than from the South, as they had prior to September.

Autospectra of the various buoy measurements revealed strong diurnal and semidiurnal variability for barometric pressure and SST and lesser variability at these periods for air temperature, wind speed, and wave height. Also, weaker synoptic variability was evident at periods of 3–4 days for most of the atmospheric parameters.

Observations at each of the buoys acquired during this study were also used to calculate the surface fluxes of latent and sensible heat. The latent heat fluxes usually far exceeded the sensible heat fluxes. The latent and sensible heat fluxes were dominated by the synoptic events which took place after mid-September. Sharp, positive maxima in the fluxes coincided with the arrival of these transient events. The predominant direction of heat transfer for both fluxes was from the ocean to the atmosphere at the buoy location furthest offshore (station 42002). However, for the buoy closer to the coast (station 42019), although the latent heat transfer was generally positive, the sensible heat transfer was directed from the atmosphere to the ocean (i.e. negative) a majority of the time.

An analysis of co-located wind wave data indicated that major heat-flux events coincided with conditions of active wave growth. However, the present data did not provide a sufficient basis to infer of any causal relationships.

Acknowledgements

We take this opportunity to thank Bhavani Balashubramaniyan and Rachel Teboulle for constructing many of the figures contained in the text. We thank Lech Lobocki and Dmitry Chalikov for providing technical assistance during the course of this study. We also thank D.B. Rao, Steve Lord, Ted Mettlach, Eric Meindl and Ed Michelena for providing reviews of the text. Finally, we thank the two anonymous reviewers for their many helpful comments.

H.L. Tolman is a UCAR Visiting Scientist.

References

Breaker, L.C., Gilhousen, D.B., Burroughs, L.D., 1997. Preliminary results from long-term measurements of atmospheric moisture in the marine boundary layer in the Gulf of Mexico. J. Atmos. Oceanic Technol. 14, in press.

Blanc, T.V., 1985. Variation of bulk-derived surface flux, stability, and roughness results due to the use of different transfer coefficient schemes. J. Phys. Oceanogr. 15, 650–669.

Coantic, M., Friehe, C.A., 1980. Slow-response humidity sensors. Air–sea interaction. In: Dobson, F., Hasse, L., Davis, R. (Eds.), Instruments and Methods. Plenum Press, New York, pp. 399–411.

Crane, J., Boole, D., 1988. Thin film humidity sensors: a rising technology. Sensors 5, 32–35.

Crescenti, G.H., Payne, R.E., Weller, R.A., 1990. Improved meteorological measurements from buoys and ships (IMET): preliminary comparison of humidity sensors. Woods Hole Tech. Rep. WHOI-90-18, Woods Hole Oceanographic Institution, 57 pp.

Crisp and Lewis, 1992.

da Silva, A.M., Young, C.C., Levitus, S. 1994. Atlas of Surface Marine Data 1994, Vol. 3: Anomalies of Heat and Momentum Fluxes. NOAA Atlas NESDIS 8, US Department of Commerce, NOAA, National Environmental Satellite, Data, and Information Service, 413 pp.

DiMego, G.J., Bosart, L.F., Endersen, G.W., 1976. An examination of the frequency and mean conditions surrounding frontal incursions into the Gulf of Mexico and Caribbean Sea. Mon. Wea. Rev. 104, 709–718.

Fairall, C.W., Edson, J.B., Miller, M.A., 1990. Heat fluxes, whitecaps, and sea spray. In: Geernaert, G.L., Plant, W.J. (Eds.), Surface Waves and Fluxes, Vol. 1, Current Theory. Kluwer Academic Publishers, Dordrecht, pp. 173–208.

Gill, A.E., 1982. Atmosphere–Ocean Dynamics, International Geophysics Series, 30, Academic Press, New York, 662 pp.

Henry, W.K., 1979. Some aspects of the fate of cold fronts in the Gulf of Mexico. Mon. Wea. Rev. 107, 1078–1082.

Hundermark, B.W., 1989. Field evaluation of the Rotronic humidity sensor and the impulsphysik visibility sensor. In: Proceedings of the Conference and Exposition on Marine Data Systems, New Orleans, Louisiana, Marine Technology Society, pp. 81–85.

IMSL, Inc. (1982) IMSL Library Reference Manual, ed. 8, Vol. 2, Houston, Texas.

Katsaros, K.B., DeCosmo, J., Lind, R.J., Anderson, R.J., Smith, D.S., Kraan, R., Oost, W., Uhlig, K., Mestayer, P.G., Larsen, S.E., Smith, M.H., de Leeuw, G., 1994. Measurements of humidity and temperature in the marine environment during the HEXOS main experiment. J. Atmos. Oceanic Technol. 11, 964–981.

Kraus, E.B., Businger, J.A. 1994. Atmosphere–Ocean Interaction, 2nd ed. Clarendon Press, Oxford, 362 pp.

List, 1966.

Muller, S.A., Beekman, P.J., 1987. A test of commercial humidity sensors for use at automatic weather stations. J. Atmos. Oceanic Technol. 4, 731–735.

Panofski, H.A., Dutton, J.A., 1984. Atmospheric Turbulence, Wiley, New York.

Phillips, O.M., 1958. The equilibrium range in the spectrum of wind-generated waves. J. Fluid Mech. 4, 426–434.

Pierson, W.J., Moskowitz, L., 1964. A proposed spectral form for fully-developed wind seas based on the similarity theory of S.A. Kitaigorodskii. J. Geophys. Res. 69, 5181–5190.

Semmer, S.R., 1987. Evaluation of a capacitance humidity sensor. In: Sixth Symposium on Meteorological Observations and Instrumentation, New Orleans, LA, American Meteorological Society, pp. 223–225.

Visscher, G.J.W., Schurer, K. 1985. Some research on the stability of several capacitive thin film (polymer) humidity sensors in practice. In: Proceedings of the 1985 International Symposium on Moisture and Humidity, Washington, DC, Instrument Society of America, pp. 515–523.

Van der Meulen, J.P., 1988. On the need of appropriate filter techniques to be considered using electrical humidity sensors. In: Proc. WMO Technical Conf. on Instruments and Methods of Observation (TECO-1988), Leipzig, Germany, WMO, pp. 55–60.

World Meteorological Organization, 1983. Measurement of Atmospheric Humidity. Guide to Meteorological Instruments and Methods of Observation, 5th ed. WMO No. 8.

Wu, J., 1974. Evaporation due to spray. J. Geophys. Res. 79, 4107–4109.

Wu, J., 1980. Wind-stress coefficients over sea surface near neutral conditions – a revisit. J. Phys. Oceanogr. 10, 727–740.